Journal of Physics:
Conference Series

PAPER • OPEN ACCESS

Rectilinear and torsional modal analysis of a drone propulsion system using optical methods

To cite this article: Cs. Horváth *et al* 2026 *J. Phys.: Conf. Ser.* **3190** 012003

Journal of Physics: Conference Series **3190** (2026) 012003 doi:10.1088/1742-6596/3190/1/012003

Rectilinear and torsional modal analysis of a drone propulsion system using optical methods

Cs. Horváth[1]*, Sz. Gungl[2], B. Istók[1], T. Kimpián[2]

[1] Department of Fluid Mechanics, Budapest University of Technology and Economics, , Faculty of Mechanical Engineering, Department of Fluid Mechanics , Budapest, Hungary
[2] System and Vehicle Dynamics Department, thyssenkrupp Components Technology Hungary Kft, Acoustics and Signal Processing Group, Budapest, Hungary

*E-mail: horvath.csaba@gpk.bme.hu

Abstract. Drone noise is a topic of increased interest in the aeroacoustics community. Typical experimental investigations apply microphone measurements to study the aeroacoustic characteristics of drone propulsion systems, often overlooking vibration-induced effects. This investigation applies rectilinear and torsional experimental modal analysis techniques to investigate a drone propulsion system. Rectilinear excitation is carried out using a traditional electrodynamic shaker, while the brushless DC motor of the propulsion system is utilized for the torsional excitation. The structure's response is recorded using a high-speed camera and analyzed with magnification algorithms. The goal of the investigation is to apply well-established experimental modal analysis methods to the new application area of drone propulsion systems to help separate vibration-induced noise sources from aerodynamically induced ones.

1. Introduction

In the aeroacoustics community, drone noise is a topic that has received increased attention. As the number of drone application areas and the number of drones have drastically increased, the resulting noise has become a relevant problem [1,2]. Therefore, a significant amount of time and resources have been invested in better understanding the noise sources of drone propulsion systems to mitigate their noise levels [1,2]. Many investigations focus on the dominant noise sources, studying the root causes and the effects of various parameters on them, such as Reynolds number [3], axial velocity [3], RPM [4], and the size and spacing of various elements [4].

A segment of the low Reynolds number acoustic investigations has focused on better understanding the coherent structures that can be generated on airfoil surfaces, referred to in the literature as profile vortex shedding [5-8].

Profile vortex shedding has been described in the literature. The classic description is in accordance with the works of Tam [9] and Wright [10], and describes it as the result of a self-excited acoustic feedback loop. An unstable laminar boundary layer on the airfoil surface results in Tollmien–Schlichting instability waves that propagate downstream toward the airfoil's trailing edge. There, sound scattering occurs, with the acoustic waves propagating back upstream to where the Tollmien–Schlichting instability waves originated in the unstable laminar boundary layer. The acoustic waves can drive the instabilities if the phase conditions are appropriate, closing the feedback loop. Profile vortex shedding is important, as it results in a periodically fluctuating force normal to the airfoil chord, being cited as one of the primary sources of aeroacoustic noise of low-speed axial flow fans [6]. Other investigations, such as the work of Ausoni et al. [11] on hydrofoils, state that the frequency of periodic vortex shedding may be influenced by periodic vibrations occurring at natural frequencies, which could result in the periodic vortex shedding being coupled to the natural frequencies of the given body, that could differ from those which would be calculated according to vortex shedding theories and models.

In the aeroacoustics community, many of the drone acoustic investigations are carried out using single microphones (as in [12]) or linear arrays of microphones (as in [4]). The microphone time signals are processed to provide sound pressure level frequency spectra. If linear arrays of microphones are processed, information can be extracted from the spectra regarding the directivity of the sound components. Utilizing such investigation methods, one can determine the occurrence of profile vortex shedding and its influence on the sound field, based on models that predict its expected Reynolds number range and frequency content [5-8]. At the same time, investigations can be found in the literature that examine the vibrations of drones [13] and their propellers [14], with only a limited number of articles appearing that investigate the possible connections between the natural frequencies of the drone propulsion systems (motor and propeller pair) and the resulting acoustic field, with [15] discussing how motor natural frequencies can radiate noise.

This investigation looks at a drone propulsion system that has been utilized on a drone aerodynamic and aeroacoustic test bench at the Budapest University of Technology and Economics. The test bench has been designed to investigate multiple drone configurations to understand their basic noise sources in greater detail, including that of a single isolated drone motor and propeller. To truly understand the measurement results and draw general conclusions, a basic understanding of the periodic vibration properties resulting from the structural natural frequencies of the drone propulsion system must first be attained. Herein, rectilinear and torsional modal analysis methods [16,17], coupled with optical evaluation techniques, have been applied to identify the structural natural frequencies and associated vibration modes of the drone propulsion system under investigation. In doing so, it has also been shown that the methods in [16] and [17] are suitable for the investigation of drone propulsion systems, extending their range of applicability to further areas of research and development.

2. Modal analysis theoretical background

This chapter provides a brief summary of the most important theoretical considerations on which the experiments have been based. Though the modes of the entire drone propulsion system (including the motor) can be investigated with this method, the focus herein is on identifying all of the important modes of the propeller. First, a brief introduction is provided on the excitation signals that have been used to identify the natural frequencies, after which a short overview is provided on the motion magnification algorithm used to capture and identify the actual vibration shapes during the sine testing.

2.1. Excitation methods

Two different excitation configurations have been utilized to acquire the in-plane and the out-of-plane modes of the drone propeller. The in-plane vibration shapes have been excited using the drone's Brushless DC (BLDC) motor, while the out-of-plane modes have been driven with an electrodynamic shaker. As the propeller may be highly inhomogeneous and anisotropic, certain modes have been excited in both cases. At the same time, differences in leading and trailing edge stiffnesses may also have demonstrated a significant effect on the results. After identifying the

Journal of Physics: Conference Series **3190** (2026) 012003 doi:10.1088/1742-6596/3190/1/012003

various potential natural frequencies, the specific modes have been excited using pure sine wave signals during image acquisition.

Rectilinear (shaker) excitation

To excite the drone propeller's out-of-plane modes, its mounting point has been excited using a standard electrodynamic shaker. The shaker has been driven by one channel of the amplifier described in Section 3.1, utilized in voltage mode. The signal used to drive the shaker has been a Schröder multisine signal [18] with fs = 48 kHz, df = 0.25 Hz, and a bandwidth from 100 – 4000 Hz, generated in MATLAB R2023b according to Eq. 1.

$$x(t) = \sum_{k=1}^{N_k} A_k \cos\left(\omega_k t + \frac{-k(k-1)\pi}{N_k}\right) \qquad (1)$$

In Eq. 1, N_k is the total number of frequency components being driven, each having an amplitude of A_k, a frequency of ω_k, and a Schröder phase of $\frac{-k(k-1)\pi}{N_k}$. The equation has been computed using an IFFT, as suggested by [19], for the fast generation of the excitation signal. The advantages of the Schröder multisine are numerous. It consists of only those sinusoids that match the analysis frequency grid, and therefore, one period of the multisine can be repeated any number of times while keeping the excitation periodic. Hence, a rectangular analysis window can be used to process the measured responses. During the actual measurements, 12 cycles of the signal have been used for each measurement. Furthermore, the excitation and the response measurement systems can run independently.

Torsional vibration excitation

In order to create broadband torsional excitation, the following three-phase Schröder multisine signal has been generated according to Eq. 2 [16]. The additional phase shift term $\frac{2\pi(i-1)}{N_{ph}}$ is introduced in order to provide the necessary alignment of the signals with the given motor topology, in this case three-phase BLDC.

$$x_i(t) = \sum_{k=1}^{N_k} A_k \cos\left(\omega_k t + \frac{-k(k-1)\pi}{N_k} + \frac{2\pi(i-1)}{N_{ph}}\right) \qquad (2)$$

$$M(t) = \frac{\hat{\Psi} p N_{ph}}{2} \sum_{k=1}^{N_k} A_k \cos\left(\omega_k t + \frac{-k(k-1)\pi}{N_k} - p\varphi_0\right) \qquad (3)$$

Eq. 3 shows the expression of the torque generated in the air-gap of the drone motor, where $\hat{\Psi}$ is the peak flux linkage, p is the number of pole-pairs, N_{ph} the number of phases, and φ_0 is the equilibrium propeller angle position around which the torsional vibration occurs [16]. It should be noted that during the torsional vibration around the equilibrium propeller angle position, the drone motor is not rotating, but only vibrating back and forth.

2.2. Image-based Modal Analysis

Traditional modal analysis of structures typically relies on accelerometers to record vibration responses. However, in the case of light structures, the addition of even a small mass sensor inherently alters the dynamic properties, shifting their natural frequencies and damping characteristics. To avoid this modal perturbation and preserve the true behavior of the propeller, non-contact measurement techniques are preferred.

One widely adopted non-contact approach is the Laser Doppler Vibrometer (LDV), which provides high-precision vibration velocity measurements across multiple discrete points on the structure. After careful optical and electronic calibration, an LDV can resolve sub-micrometer motion, enabling quantitative modal identification [20]. Despite its accuracy, LDV scanning is inherently a point-by-point process, which can be time-consuming when characterizing complex mode shapes over an entire propeller surface.

Various signal processing methods are utilized in image-based modal analysis and vibration measurements. Digital Image Correlation (DIC) is a well-known technique for displacement and strain measurement of speckled specimens [21]. Subpixel registration can be performed by fitting a curve to the integer pixel correlation coefficients and using the peak of this fitted curve to determine the subpixel displacement [22]. This method, when combined with integer pixel correlation calculations in the Fourier domain, is relatively fast but does not provide the highest accuracy. Alternatively, subpixel displacements can be determined iteratively using a root-finding method such as Newton-Raphson. This approach involves interpolating the subset and calculating the correlation until the desired convergence is reached. Although the Newton-Raphson method enhances accuracy, it requires more processing time [23]. Furthermore, 3D point tracking [24] and phase-based optical flow techniques [25] have also been successfully used in full-field modal analysis. Differential optical flow methods, such as the Lucas-Kanade method [26] (which can be thought of as the general form of DIC, point tracking, and phase-based methods), and the Horn-Schunck algorithm [27], are typically used in real-time operations.

Phase-based motion magnification

During product development, qualitative analysis can also be invaluable. For instance, a clear and intuitive video of a complex, hard-to-model assembly vibrating in a specific mode shape can provide significant insights for mechanical engineers designing intricate systems. Phase-based motion magnification [28] builds on this concept by decomposing each video frame into a multiscale, multi-orientation pyramid of spatial frequency bands. The local phase of each band, which encodes sub-pixel positional information, is extracted and passed through a temporal band-pass filter tuned to the frequency of interest. By amplifying the filtered phase signal and reconstructing the frames, a magnified visualization of the motion at that specific frequency can be obtained. This approach enhances sensitivity to sub-pixel vibrations while attenuating uncorrelated noise and lighting changes, making it well-suited for structural dynamics applications.

Subsampling method

Traditionally, high-speed cameras are required for measuring a sufficient frequency range for analysis. However, most commercially available and affordable cameras can only record at 60-90 fps at full resolution, although this can be higher if the number of recorded pixel rows is decreased. Some techniques have been developed to record temporally aliased signals and reconstruct the original signal with minimal information loss [29]. In the present study, drone propeller modal shapes are excited sequentially at each resonance frequency, as determined by Schröder multi-sine measurement. For each target mode, the propeller is driven at a single harmonic frequency while a high-speed camera captures the resulting motion. To ensure a smooth temporal representation of each oscillation, the sampling rate must exceed ten times the excitation frequency. The Phantom VEO 640 camera used herein supports up to 20,000 frames per second (fps) at a resolution of 1920 x 200, limiting direct measurement to modes below 2,000 Hz. To extend the measurable bandwidth, we exploit controlled aliasing: by selecting a frame rate slightly offset — either 0.9 or 1.1 times the mode frequency — the aliased signal falls into the low-frequency baseband that still meets the 10x oversampling requirement. Post-processing then applies a narrowband temporal filter to isolate each aliased component before phase amplification, yielding clear, quantitative visualizations of the propeller's dynamic mode shapes.

Journal of Physics: Conference Series **3190** (2026) 012003 doi:10.1088/1742-6596/3190/1/012003

3. Measurement setup

This section describes the experimental setup for the broadband and narrowband measurements, which have been used to first localize the natural frequencies and then capture the individually excited vibration shapes.

3.1. Excitation signal amplifier

Fig. 1 shows the current feedback amplifier's schematic circuit diagram used to excite the shaker in "Voltage Mode" and the stator of the drone motor in "Current Mode" [17]. Following the signal path, the operation is as follows. An IC1 industrial differential amplifier receives the input signal on its non-inverting input and, depending on the state of the "Voltage / Current Mode" switch, it works as a gain stage in "Voltage Mode" or as an error amplifier in "Current Mode", subtracting the output of the HX05-NP current transducer from the input signal. Furthermore, it sets the loop gain with its 20 dB voltage amplification factor. The power stage is built around IC_2, which is an industrial power operational amplifier, providing the necessary output current and an additional 12 dB gain. R_s protects IC_2 from operating in "almost short-circuit" condition, as the typical DC resistances of drone motors are a few times 10 mΩs. The first-order low-pass filter, consisting of R_5 and C_1, models the -3 dB bandwidth of the current transducer, as it is modelled by a current-voltage converter in TINA-TI.

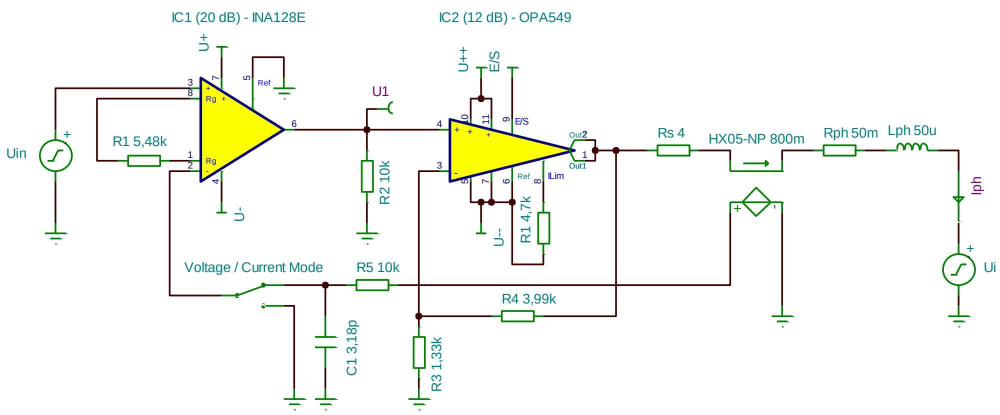

Figure 1. Schematic of one channel of the voltage / current output amplifier used to excite the shaker (Voltage Mode) and the stator of the drone motor (Current Mode).

3.2. Acoustic measurement of natural frequencies

Fig. 2 shows the measurement setup with which the natural frequencies of the propeller (T-Motor P15*5 Propeller) have been determined using the torsional excitation generated with the drone motor (T-Motor MN4010). For this, the drone motor has been placed in a fixed position (no rotation), and the stator has been driven with a three-phase Schröder multisine current, as described in Section 2.1. and the radiated nearfield sound pressure has been recorded using a ¼" measurement microphone (GRAS 40 PP 10 type) and recorded using a National Instruments DAQ card (NI-9234).

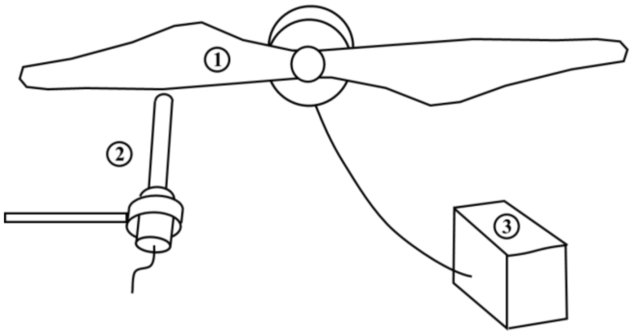

Figure 2. Nearfield radiated noise measurement used to determine the natural frequencies appearing by torsional excitation. Motor and propeller (1), Microphone (2), electrical excitation (3). A similar setup has been used in conjunction with the shaker setup.

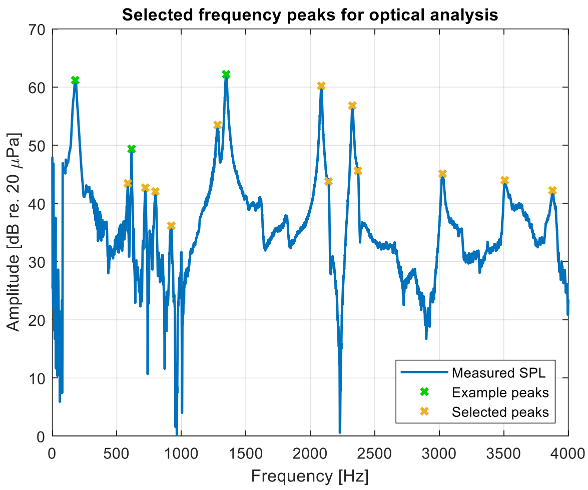

Figure 3. The spectrum of the nearfield sound pressure with torsional excitation from the drone motor and the peaks selected for optical analysis. The green crosses depict two out-of-plane and one in-plane modes of the propeller.

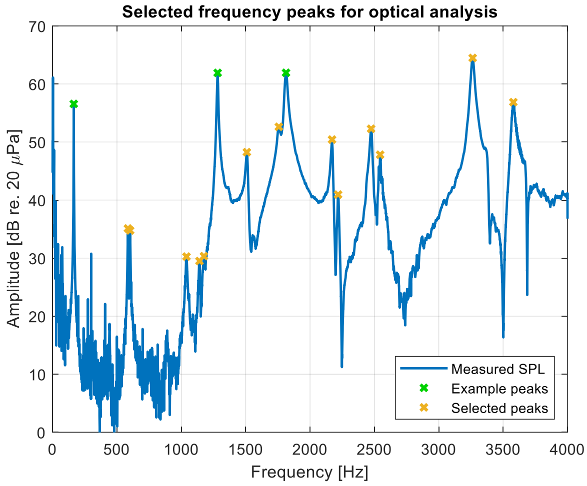

Figure 4. The spectrum of the nearfield sound pressure with rectilinear excitation and the frequency peaks selected for optical analysis. The green crosses depict the first three bending modes shown in Figs. 6-11.

A very similar setup has been utilized to acquire the natural frequencies using the electrodynamic shaker described in Section 2.1. To summarize the results, Figs. 3 and 4 show the averaged spectra of the recorded response, with the analyzed peaks being marked with an 'x' for torsional and rectilinear excitation, respectively. The averaged spectra have been computed in MATLAB R2023b using Welch's method [30] with the following parameters: fs = 51.2 kHz, df = 0.25 Hz, Rectangular window, 8 averages, and 0 % overlap, as the excitation signal is exactly periodic within the analysis window.

3.3. *Optical measurement of natural frequencies*

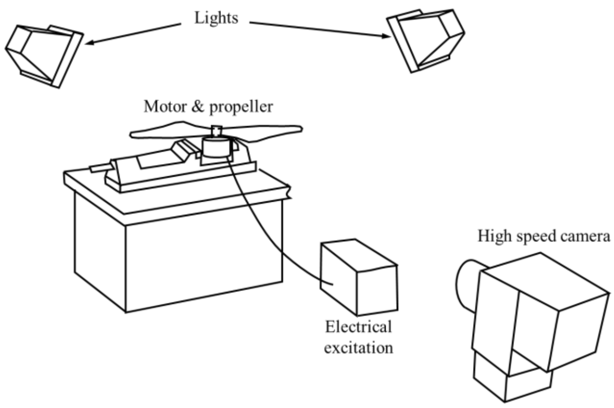

Figure 5. Optical measurement setup

Journal of Physics: Conference Series **3190** (2026) 012003 doi:10.1088/1742-6596/3190/1/012003

Once the natural frequencies have been identified, pure sine wave excitation has been applied to study each potential mode shape of the propeller for each excitation configuration. In this way, the in-plane and out-of-plane modes have been excited one by one and recorded using an appropriate sampling rate with the high-speed camera (Phantom VEO 640) (taking into consideration the necessary subsampling rate, where necessary). During the measurement, the necessary illumination has been provided with non-flickering spotlights. It is noted that the stiffening effects associated with the rotation of the drone propulsion system (during normal rotational operation) have not yet been accounted for herein and will be examined during a later phase of the investigation, which is beyond the scope of this paper.

4. Experimental results

We have recorded short movies for all the selected peaks in Figs. 3 and 4 in order to understand whether the amplified response has truly been caused by an excited mode of the propeller or some other phenomena in the examined system (for example, a resonance of the motor or the mounting). In this section, we present a few examples (marked in green in the spectra in Figs. 3 and 4) of vibration shapes for rectilinear and torsional excitation.

4.1. Mode shapes with rectilinear excitation

Figs. 6 and 7 show the first out-of-plane bending mode of the propeller @ 177.25 Hz for the shaker setup. The figures depict the bending phenomenon by simultaneously presenting three overlapped layers: the static propeller geometry and two maxima of motion, presented with the help of two different color semi-transparent layers. Fig. 7 is a magnified view of the right side of the propeller, where the displacement of the tip is significant, and therefore easiest to recognize.

Figure 6. First out-of-plane bending mode of the propeller @ 177.25 Hz

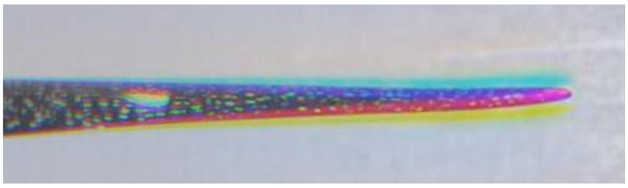

Figure 7. Magnified view of the blade tip for the first out-of-plane bending mode of the propeller @ 177.25 Hz

Figs. 8 and 9 and Figs. 10 and 11 are of the second and the third out-of-plane bending modes, respectively. The nodes can be clearly seen thanks to the coloring.

Journal of Physics: Conference Series **3190** (2026) 012003 doi:10.1088/1742-6596/3190/1/012003

Figure 8. Second out-of-plane bending mode of the propeller @ 614.5 Hz

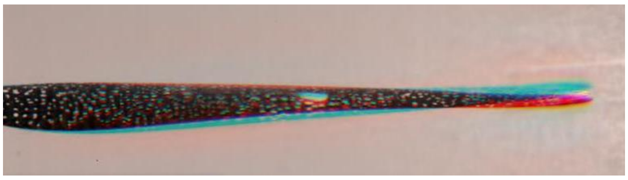

Figure 9. Magnified view of the blade tip in the second out-of-plane bending mode of the propeller @ 614.5 Hz. The node of the vibration shape is clearly visible

Figure 10. Third out-of-plane bending mode of the propeller @ 1347.5 Hz

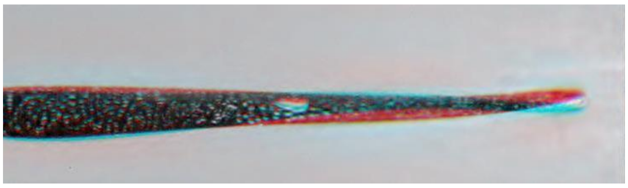

Figure 11. Magnified view of the blade tip in the third out-of-plane bending mode of the propeller @ 1347.5 Hz. The two nodes of the vibration shape are clearly visible.

4.2. Mode shapes with torsional excitation

As expected in advance, some signs of coupling between out-of-plane modes and the in-plane excitation have been noticed. A perfect example can be seen in Fig. 12, where the first bending mode is excited although the excitation of the propeller has been purely torsional. However, instead of 177.25 Hz, this mode appears @164.5 Hz, which is most likely due to the different mounting and excitation conditions.

Figure 12. First out-of-plane bending mode of the propeller @ 164.5 Hz

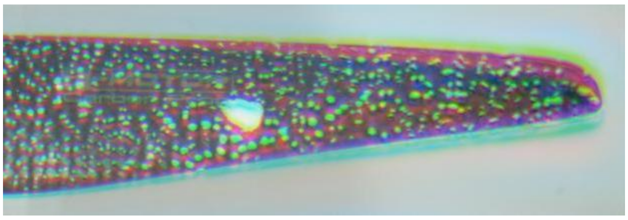

Figure 13. Magnified view of the blade tip for the first out-of-plane bending mode of the propeller @ 164.5 Hz. This mode also appears in the shaker measurements, however, at a slightly different frequency.

Fig. 14 shows the third out-of-plane bending mode excited with pure in-plane excitation @ 1282.25 Hz. These mode shapes could be visualized better from a tilted view, as they are hardly visible in 2D from a top view.

Figure 14. Third out-of-plane bending mode of the propeller @ 1282.25 Hz

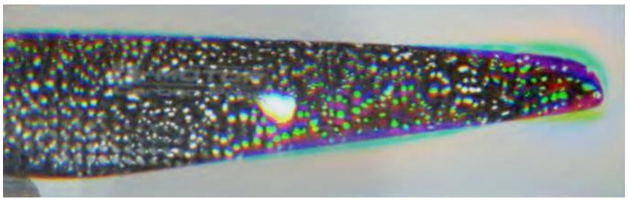

Figure 15. Magnified view of the blade tip in the third out-of-plane bending mode of the propeller @ 1282.25 Hz. The two nodes of the vibration shape are clearly visible. The excitation has been purely in-plane.

Fig. 16 shows the propeller from a top view and provides an example for an in-plane mode @ 1813.5 Hz. The magnified view in Fig. 17 highlights the in-plane motion of the blade tip.

Figure 16. Example of an in-plane bending mode of the propeller @ 1813.5 Hz

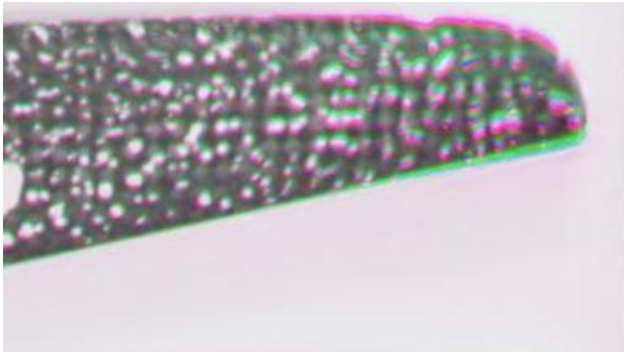

Figure 17. In-plane motion of the propeller @ 1813.5 Hz

5. Conclusions

This paper presents the modal analysis of a drone propulsion system using torsional and rectilinear excitation methods coupled with phase-based motion magnification and subsampling methods. The application of these methods in the investigation of drone propulsion systems has proven successful, as the various modes of the drone propulsion system could be excited and clearly identified. Though the entire drone propulsion system (motor and propeller) could be investigated in this manner, here the focus has been on identifying the in-plane and out-of-plane modes of the propeller. The results presented herein lay the foundation for the comprehensive modal analysis of the entire drone propulsion system, which will be carried out in the next step of the investigation.

Once all the modes of the motor and propeller have been identified, the attained modes will be compared to acoustic modes identified during microphone measurements of the drone propulsion system, recorded under run-up operating conditions on the drone test bench. Current assumptions in the industry suggest that when profile vortex shedding leads to aerodynamic noise, it is a result of self-excited acoustic feedback loops. Comparing the modal analysis data with the acoustic data, and further theoretical considerations regarding the generation of profile vortex shedding, it will be investigated whether periodic vibrations at natural frequencies of the drone propulsion system could potentially instigate and/or amplify such noise sources under certain design and operating conditions. The long-term goal of the investigation is to provide design guidelines on behalf of engineers to help them avoid design and operating conditions that could lead to the instigation and/or further amplification of excess noise.

6. Acknowledgements

This collaboration has been a fruitful non-profit partnership for the sake of advancing knowledge and personal growth through mutual learning and experience exchange. We are grateful for the opportunity and support provided by Budapest University of Technology and Economics and thyssenkrupp Components Technology Hungary Ltd. The colleagues from the Department of Fluid Mechanics have been supported by the János Bolyai Research Scholarship of the Hungarian Academy of Sciences, and project no. 143204, implemented with the support provided by the Ministry of Innovation and Technology of Hungary from the National Research, Development and Innovation Fund, financed under the OTKA K 22 funding scheme, while a portion of the equipment has been provided by the European Union and the Hungarian Government in the framework of Competitive Central-Hungary OP (Project ID: VEKOP-2.3.3-15-2017-00017).

References

[1] Y. Liua, M. Kreimeier, E. Stumpf, Y. Zhou, and H. Liu, *Overview of Recent Endeavors on Personal Aerial Vehicles: A Focus on the US and Europe led Research Activities*, Progress in Aerospace Sciences, 2017, Vol. 91, pp. 53-66, https://doi.org/10.1016/j.paerosci.2017.03.001.

[2] C. Yang, R. J. Wallace, and C. A. Huang, *Review and Bibliometric Analysis of Unmanned Aerial System (UAS) Noise Studies Between 2015 and 2024*, Acoustics, 2024, 6, 997-1020, https://doi.org/10.3390/acoustics6040055.

[3] D. Casalino, E. Grande, G. Romani, D. Ragni, and F. Avallone, *Definition of a benchmark for low Reynolds number propeller aeroacoustics*, Aerospace Science and Technology, 2021, Volume 113, 106707, ISSN 1270-9638, https://doi.org/10.1016/j.ast.2021.106707.

[4] R. S. McKay, M. J. Kingan, S. T. Go, and R. Jung, *Experimental and analytical investigation of contra-rotating multi-rotor UAV propeller noise*, Applied Acoustics, 2021, Volume 177, 107850, ISSN 0003-682X, https://doi.org/10.1016/j.apacoust.2020.107850.

[5] G. Daku, and J. Vad, *Experiment-Based Preliminary Design Guidelines for Consideration of Profile Vortex Shedding From Low-Speed Axial Fan Blades*, JOURNAL OF TURBOMACHINERY-TRANSACTIONS OF THE ASME, 2021, 143 : 6 Paper: 061014 , 10 p., https://doi.org/10.1115/1.4050392.

[6] G. Daku, and J. Vad, *Preliminary Design Guidelines for Considering the Vibration and Noise of Low-Speed Axial Fans Due to Profile Vortex Shedding*, INTERNATIONAL JOURNAL OF TURBOMACHINERY PROPULSION AND POWER, 2022, 7 : 1 p. 2 , 23 p., https://doi.org/10.3390/ijtpp7010002.

[7] E. Balla, and J. Vad, *Refinement of a semi-empirical method for the estimation of profile vortex shedding frequency from low-speed axial fan blade sections*, In: The European Turbomachinery Society (Euroturbo) Proceedings of 14th European Conference on Turbomachinery Fluid dynamics & Thermodynamics ETC14, Gdansk, Poland, April 12-16, 2021, Paper: ETC2021-591 , 12 p.

[8] G. Daku, and J. Vad, *A Comprehensive Analytical Model for Vortex Shedding from Low-Speed Axial Fan Blades*, JOURNAL OF TURBOMACHINERY-TRANSACTIONS OF THE ASME, 2023, 145 : 7 Paper: 071008 , 11 p., https://doi.org/10.1115/1.4056700.

[9] C. K. W. Tam, *Discrete tones of isolated airfoils*, J. Acoust. Soc. Am. 1974, 55, 1173–1177, https://doi.org/10.1121/1.1914682.

[10] S. Wright, *The acoustic spectrum of axial flow machines*, J. Sound Vib. 1976, 45, 165–223, https://doi.org/10.1016/0022-460X(76)90596-4.

[11] P. Ausoni, M. Farhat, Y. Bouziad, J.-L. Kueny, F. Avellan, *Kármán vortex shedding in the wake of a 2D hydrofoil: Measurement and numerical simulation*, In Proceedings of the IAHR International Meeting of WG on Cavitation and Dynamic Problems in Hydraulic Machinery and Systems, Barcelona, Spain, June 28–30, 2006; p. 14. Available online: https://infoscience.epfl.ch/record/88122 (accessed on April 26, 2025).

[12] G. Yakhina, M. Roger, S. Moreau, L. Nguyen, V. Golubev, *Experimental and Analytical Investigation of the Tonal Trailing-Edge Noise Radiated by Low Reynolds Number Aerofoils*, Acoustics, 2020, 2, 293–329, https://doi.org/10.3390/acoustics2020018.

[13] K. Chen, W. Meng, J. Wang, K. Liu, Z. Lu, *An investigation on the structural vibrations of multi-rotor passenger drones*, International Journal of Micro Air Vehicles, 2023, 15, doi:10.1177/17568293231199097.

Journal of Physics: Conference Series **3190** (2026) 012003 doi:10.1088/1742-6596/3190/1/012003

[14] M.-R. Ashory, F. Talebi, H. R. Ghadikolaei, M. Karimpour, *Investigating the vibrational behaviour of a rotating two-blade propeller by using a self-tracking method*, Proceedings of the Institution of Mechanical Engineers, Part C., 2018, 233 (3), 835-847, doi:10.1177/0954406218764514.
[15] J. D. Cluts, B. S. Henderson, and E. Pierson, *An Initial Electric Motor Rotor Vibration Model*, AIAA SCITECH 2024 Forum, Orlando, FL, January 8-12, 2024, AIAA 2024-2302, https://doi.org/10.2514/6.2024-2302.
[16] T. Kimpián, F. Augusztinovicz, *Universal broadband torsional exciter from a permanent magnet synchronous motor*, Proceedings of ISMA2014-USD2014, International Conference on Noise and Vibration Engineering, September 15-17, 2014, Leuven, Belgium, pp. 1101-1109, ISBN 978-16-343950-6-9.
[17] T. Kimpián, F. Augusztinovicz*, Torsional modal analysis made easy – Methodology and practical examples from electric motor testing*, Proceedings of ISMA2022-USD2022, International Conference on Noise and Vibration Engineering, September 12-14, 2022, Leuven, Belgium, pp. 4187-4201, ISBN 978-90-828931-5-1.
[18] M. A. Schröder, *Synthesis of low peak-factor signals and binary sequences of low autocorrelation*, IEEE Transactions on Information Theory, 1970, vol. 16, pp. 85–89, DOI: 10.1109/TIT.1970.1054411.
[19] R. Pintelon, J. Schoukens, *System Identification – A Frequency Domain Approach*, IEEE Press, The Institute of Electrical and Electronics Engineers, New York, 2001, ISBN 0-7803-6000-1.
[20] J. Baqersad, P. Poozesh, C. Niezrecki, and P. Avitabile, *Photogrammetry and optical methods in structural dynamics – a review*, Mechanical Systems and Signal Processing, 2017, vol. 86, pp. 17–34, https://doi.org/10.1016/j.ymssp.2016.02.011.
[21] M. A. Sutton, J. J. Orteu, and H. Schreier, *Image correlation for shape, motion and deformation measurements: basic concepts, theory and applications*. Springer Science & Business Media, New York, 2009, ISBN 978-0-387-78747-3.
[22] J. Javh, J. Slavič, and M. Boltežar, *The subpixel resolution of optical-flow-based modal analysis*, Mechanical Systems and Signal Processing, 2017, vol. 88, pp. 89–99, 05, http://dx.doi.org/10.1016/j.ymssp.2016.11.009.
[23] P. Bing, X. Hui-min, X. Bo-qin, and D. Fu-long, *Performance of sub-pixel registration algorithms in digital image correlation*, Measurement Science and Technology, 2006, vol. 17, 1615, DOI 10.1088/0957-0233/17/6/045.
[24] P. Olaszek, *Investigation of the dynamic characteristic of bridge structures using a computer vision method*, Measurement, 1999, vol. 25, no. 3, pp. 227–236, https://doi.org/10.1016/S0263-2241(99)00006-8.
[25] D. Fleet, and A. Jepson, *Computation of component image velocity from local phase information*, International Journal of Computer Vision, 1990, vol. 5, pp. 77–104, DOI https://doi.org/10.1007/BF00056772.
[26] B. D. Lucas, and T. Kanade, *An iterative image registration technique with an application to stereo vision*, In International Joint Conference on Artificial Intelligence, 1981, https://api.semanticscholar.org/CorpusID:2121536.
[27] B. Horn, and B. Schunck, Determining optical flow, Artificial Intelligence, 1981, vol. 17, pp. 185–203, https://doi.org/10.1016/0004-3702(81)90024-2.
[28] N. Wadhwa, M. Rubinstein, F. Durand, and W. T. Freeman, *Phase-based video motion processing*, ACM Trans. Graph., 2013, vol. 32, no. 4, https://doi.org/10.1145/2461912.246196.
[29] Y. Yang, C. Dorn, T. Mancini, Z. Talken, S. Nagarajaiah, G. Kenyon, C. Farrar, and D. Mascare˜nas, *Blind identification of full-field vibration modes of output-only structures from uniformly-sampled, possibly temporally-aliased (sub-nyquist), video measurements*, Journal of Sound and Vibration, 2017, vol. 390, pp. 232–256, https://doi.org/10.1016/j.jsv.2016.11.034.
[30] P. D. Welch, *The use of Fast Fourier Transform for the estimation of power spectra: A method based on time averaging over short, modified periodograms*, IEEE Transactions on Audio and Electroacoustics, 1967, AU-15 (2): pp. 70–73, doi:10.1109/TAU.1967.1161901.